International Geology Review
Publication details, including instructions for authors and subscription information:
http://www.tandfonline.com/loi/tigr20

Zircon U-Pb and pyrite Re-Os age constraints on pyrite mineralization in the Yinjiagou deposit, China

Ming-Tian Zhu[a], Lian-Chang Zhang[a], Guang Wu[b], Xin-Di Jin[a], Peng Xiang[a] & Wen-Jun Li[a]
[a] Key Laboratory of Mineral Resources, Institute of Geology and Geophysics, Chinese Academy of Sciences, Beijing, 100029, China
[b] Institute of Mineral Resources, Chinese Academy of Geological Sciences, Beijing, 100037, China
Published online: 08 Apr 2013.

To cite this article: Ming-Tian Zhu, Lian-Chang Zhang, Guang Wu, Xin-Di Jin, Peng Xiang & Wen-Jun Li (2013) Zircon U-Pb and pyrite Re-Os age constraints on pyrite mineralization in the Yinjiagou deposit, China, International Geology Review, 55:13, 1616-1625, DOI: 10.1080/00206814.2013.786313

To link to this article: http://dx.doi.org/10.1080/00206814.2013.786313

International Geology Review, 2013
Vol. 55, No. 13, 1616–1625, http://dx.doi.org/10.1080/00206814.2013.786313

Taylor & Francis
Taylor & Francis Group

Zircon U–Pb and pyrite Re–Os age constraints on pyrite mineralization in the Yinjiagou deposit, China

Ming-Tian Zhu[a], Lian-Chang Zhang[a]*, Guang Wu[b], Xin-Di Jin[a], Peng Xiang[a] and Wen-Jun Li[a]

[a]*Key Laboratory of Mineral Resources, Institute of Geology and Geophysics, Chinese Academy of Sciences, Beijing 100029, China;* [b]*Institute of Mineral Resources, Chinese Academy of Geological Sciences, Beijing 100037, China*

(*Accepted 11 March 2013*)

We report new zircon U–Pb and pyrite Re–Os geochronological studies of the Yinjiagou poly-metallic deposit, sited along the southern margin of the North China Craton (SMNCC). In this deposit, pyrite, the most important economic mineral, is intergrown/associated with Mo, Cu, Au, Pb, Zn, and Ag. Prior to our new work, the age of chalcopyrite–pyrite mineralization was known only from its spatial relationship with molybdenite mineralization and with intrusions of known ages. The U–Pb and Re–Os isotope systems provide an excellent means of dating the mineralization itself and additionally place constraints on the ore genesis and metal source. Zircons separated from the quartz–chalcopyrite–pyrite veins include both detrital and magmatic groups. The magmatic zircons confine the maximum age of chalcopyrite–pyrite mineralization to 142.0 ± 1.5 Ma. The Re–Os results yield an age of 141.1 ± 1.1 Ma, which represents the age of the chalcopyrite–pyrite mineralization quite well. The common Os contents are notably low (0.5–20.1 ppt) in all samples. In contrast, the Re contents vary considerably (3.0–199.2 ppb), most likely depending on intensive boiling, which resulted in an increase of Re within the pyrite. This study demonstrates that the main chalcopyrite–pyrite mineralization occurred late in the magmatic history and was linked to a deeper intrusion involving dominant mantle-derived materials. This mineralization event might be related to the Early Cretaceous lithospheric destruction and thinning of the SMNCC.

Keywords: zircon U–Pb dating; Re–Os isotopic age; pyrite; Yinjiagou deposit; southern margin of the North China Craton

Introduction

Precise age measurements of hydrothermal mineral deposits provide constraints on the temporal relationship of mineralization to magmatic, metamorphic, or tectonic events, and hence potentially to the origin and genesis of the ore-forming system. However, isotopic dating of metallogenic events in individual ore deposits is often difficult due to a lack of suitable minerals that can be dated precisely.

Zircon is the most widely used material for U–Pb dating of magmatic events, with a closure temperature greater than 900°C and a notably low diffusivity of U, Th, and Pb in most geological environments (Lee *et al*. 1997; Cherniak and Watson 2001). Since the 1990s, hydrothermal zircons have been found in hydrothermal minerals such as quartz, garnet, and others from many localities (Rubin *et al*. 1989; Kerrich and King 1993; Li *et al*. 1997; Hu *et al*. 2004; Hoskin 2005; Pettke *et al*. 2005; Lawrie *et al*. 2007; Pelleter *et al*. 2007; Fu *et al*. 2009; Wan *et al*. 2012), and they are sometimes used for dating of hydrothermal events. The criteria used to distinguish among them remain ambiguous.

Recent application of the Re–Os geochronometer to sulphide minerals has increasingly been used to date and trace the sources of metals in ore deposits, because of the direct association of rhenium and osmium with ore mineralization. Many studies have focused on molybdenite (e.g. Stein *et al*. 2001; Selby *et al*. 2002; Wu *et al*. 2011) because it contains high concentrations of Re and no initial Os. However, the Re–Os method also has been applied to sulphides with low Re and Os abundances, i.e. pyrite and chalcopyrite, to yield geochronological information (Stein *et al*. 1998; Mathur *et al*. 1999; Stein *et al*. 2000; Arne *et al*. 2001; Kirk *et al*. 2002; Zhang *et al*. 2005; Feng *et al*. 2009). In certain contexts, it has been shown that the Re content of pyrite can be fairly high (Stein *et al*. 2000; Morelli *et al*. 2004).

The Yinjiagou poly-metallic deposit is located in the southern margin of the North China Craton (SMNCC) (Figure 1A), where the Mesozoic intrusions clustered in the Late Jurassic–Early Cretaceous periods (e.g. Li *et al*. 2007; Mao *et al*. 2011; and references therein) control the occurrences of porphyry (skarn) Mo deposits and outlying

*Corresponding author. Email: lczhang@mail.iggcas.ac.cn

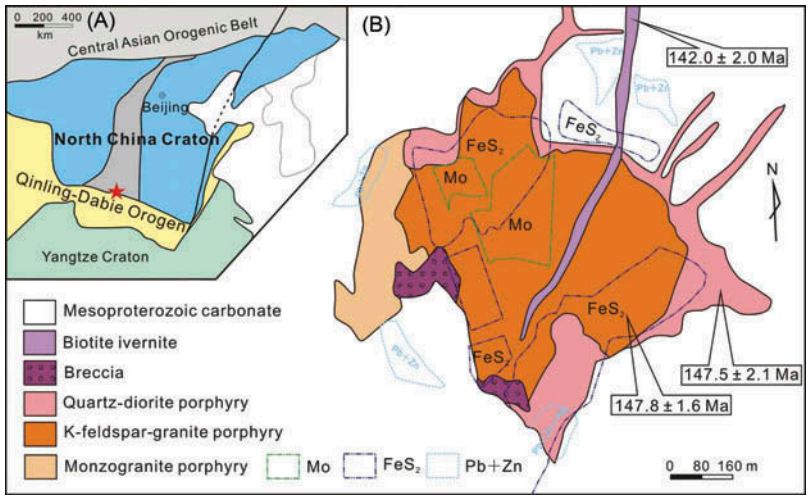

Figure 1. Tectonic location (A) and geological (B) maps of the Yinjiagou deposit on the southern margin of the North China Craton. The zircon SHRIMP U–Pb ages of the intrusions are taken from Li *et al*. (2013b).

poly-metallic veins at the deposit scale. Pyrite is the most economic mineral in the Yinjiagou deposit. The age of the pyrite mineralization is inferred only from its spatial relationship with molybdenite mineralization of known Re–Os age, and therefore, the genetic relationships between the porphyry Mo and the veined pyrite remain unclear. This article presents the dating results for zircon U–Pb and pyrite Re–Os, demonstrating the age of the pyrite mineralization and providing certain constraints on the metal source and genetic model.

Geology

The Yinjiagou deposit is tectonically located at the SMNCC. The basement of the area is the late Archaean (ca. 2.9–2.6 Ga) Taihua Group (Zhang *et al*. 2001), consisting of gneiss, granulite, and migmatite, which is disconformably overlain by the Mesoproterozoic Xiong'er Group volcanics. The overlying strata are Mesoproterozoic littoral clastic rocks and carbonate rocks of the Guandaokou Group in addition to the Neoproterozoic shallow-marine facies clastic and carbonate rocks of the Luanchuan Group. Cambrian and Lower Ordovician clastic and carbonate rocks are also extensively developed, whereas Upper Ordovician to lower Carboniferous rocks are absent. Middle–upper Carboniferous and Permian terrigenous clastic rocks, Triassic clastic rocks of alluvial and fluvial facies, Jurassic continental strata, and Cretaceous volcano-sedimentary rocks all sporadically outcrop in this area as well.

In the area of Yinjiagou, the oldest strata consist of Mesoproterozoic dolomite with interbedded chert. The NEE-trending Yechangping–Yinjiagou faults and WE-trending Jizhang–Shipo faults pass through the mining area. The Yanshanian intrusive complex (Figure 1B), emplaced at 148 to 142 Ma (Li *et al*. 2013b), is composed of monzogranite porphyry, K-feldspar-granite porphyry (KGP), quartz-diorite porphyry (QDP), and biotite ivernite, belonging to the deep-hypabyssal granites (Chen and Fu 1992; Lu *et al*. 2002). Based on the latest zircon SHRIMP U–Pb dating and field relationships, the earliest monzogranite porphyry is located to the west of the complex. The KGP containing monzogranite breccia is located in the centre of the complex, and rhyolitic tuff and explosive breccia are locally distributed around the KGP. The QDP surrounds the north, east, and south margins of the KGP. Zhang *et al*. (2008) considered that the QDP is the marginal face of the KGP without any obvious boundary line. The latest biotite ivernite cuts through all of the above-mentioned intrusions. Multiple mineralization stages developed and formed various mineralization veins (Figure 1B). The veinlet molybdenite occurs within the KGP and the pyrite–quartz ± chalcopyrite veins are several metres to tens of metres in thickness, located in the KGP and QDP and locally throughout the molybdenite ore-bodies. Quartz–Pb, Zn, and Ag veins are mainly distributed in the faults and the interstratified cracks of dolomite, especially at the junctions of two fractures, and can extend to several kilometres around the intrusions. Further details of these mineralizations are described by Chen and Fu (1992), Zhang *et al*. (2008), and Zhu *et al*. (2013). This study focuses on the pyrite mineralization.

Samples and analytical methods

The measurements were performed on representative samples of pyrite collected at different levels in the chalcopyrite–pyrite ore-bodies from underground works. The selected samples are composed of pyrite–quartz ± chalcopyrite ± calcite assemblages (Figure 2), and the size

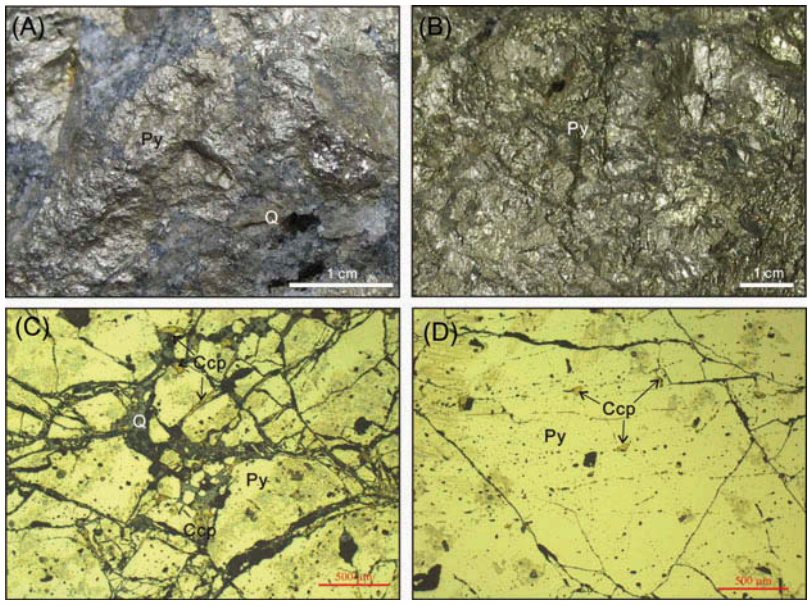

Figure 2. Typical photographs of samples from the Yinjiagou deposit. The ores consist of quartz ± pyrite in the hand specimens (A and B). The micron-size chalcopyrite occurs along the quartz veinlets (C) or in the pyrite grains (D) under reflected light.

of the pyrite grains varies between 0.1 and 10 mm. The chalcopyrite occurs along the quartz veinlets or in the pyrite grains.

The samples of pyrite–quartz ± chalcopyrite veins for U–Pb analysis were broken into fist-sized pieces. The zircon grains were separated via a combination of heavy liquid and magnetic techniques, handpicked and subsequently mounted in epoxy resin, and polished to remove the upper one-third of the grains. The mounts were vacuum-coated with high-purity gold prior to SIMS analysis. Cathodoluminescence (CL) and back-scattered electron (BSE) images were obtained based on LEO1450VP SEM to identify internal structures and choose the potential target sites for U–Pb analysis. Zircon U–Pb analyses were carried out on the Cameca IMS-1280 large-radius SIMS instrument at the Institute of Geology and Geophysics, Chinese Academy of Sciences (IGGCAS). Detailed analytical procedures can be found in Li *et al*. (2010). The analysed ellipsoidal spot size is approximately 20 × 30 μm in size. For relatively young minerals, the ages are usually calculated from the $^{206}Pb/^{238}U$ ratios, and hence, the ^{206}Pb correction method is less used for the Phanerozoic minerals. The ^{204}Pb and ^{207}Pb correction methods were prevalent for individual analyses, and an average $^{206}Pb/^{238}U$ age with a 2σ or 95% confidence level was calculated using ISOPLOT 3.0 software (Ludwig 2003).

Four pyrite mineral separates were produced via rough crushing and subsequent handpicking of pyrite grains of approximately 40–60 mesh-size fractions. These samples were divided into one or two fractions, yielding a total of six samples. All Re–Os chemical analyses were performed at the Re–Os Laboratory in the Key Laboratory of Mineral Resources, IGGCAS. The ^{185}Re and ^{190}Os spikes were provided by Oak Ridge National Laboratory. The samples were determined by the isotope dilution method. First, the pyrite samples were crushed and grounded to <200 mesh using contamination-free equipment. Approximately 1 g of samples were weighed and loaded into a Carius tube; an aliquot of 6 ml of sub-boiled HCl, together with ^{85}Re and ^{190}Os mixed spikes and 18 ml of sub-boiled HNO_3, was added to the Carius tubes, which were immersed in an ethanol–liquid–nitrogen slush. The samples were decomposed at 220°C for 48 hours. After cool-down, the Carius tubes were opened while immersed in the slush. A volume of approximately 1.5 times Milli-Q water was added to the open Carius tubes and sealed with perforated rubber heads. Two Teflon capillaries pierced in advance through the two holes in the perforated rubber head were inserted into the Carius tube and the ampoule, respectively. The Os in the sample solution was separated by distillation in the steam bath, and the resulting trapping solution collected in the ampoule was used for Os measurement. Rhenium was separated by an AG 1 × 8 anion exchange resin (100–200 mesh), and the Re and Os isotopic compositions of pyrite were measured by a Thermo Scientific ELEMENT 1 ICP-MS instrument. The intensity of the ^{190}Os signal was monitored to correct for traces of Os in the Re solution, and the ^{185}Re intensity was monitored to correct for traces of Re in the Os solution. A 3% HNO_3 solution and 30% H_2O_2 solution were used to wash the Teflon injection tube, to avoid cross-contamination between different samples during determination of the Os isotope composition. The details of the chemistry and measurement procedures are described by Jin *et al*. (2010). Our blank values were

0.42 ± 0.15 pg for Os with 0.26 ± 0.05 for $^{187}Os/^{188}Os$ and 2.0 ± 0.6 pg for Re ($n = 4$).

Results

Petrography and U–Pb dating of zircons

Zircons in the pyrite–quartz ± chalcopyrite are generally relatively coarse, with average lengths of 100 μm. Most grains are euhedral to subhedral, with few relatively rounded grains present. Most aspect ratios are mostly approximately 2:1. The prismatic faces tend to be simple in contrast to the grain terminations, which are complexly faceted. Based on the petrography and dating results, two groups of zircons were recognized: one as the older detrital zircon with scattered ages (Group A) (Figure 3A) and the other as the younger zircon with relatively concentrated ages (Group B) (Figure 3B).

The group A samples are dominantly subhedral. The CL images reveal different and complex textures, with various levels of luminescence, indicating the different sources and consistent with U–Pb ages ranging from 169 to 2740 Ma (Table 1 and Figure 4A). The group B samples examined by the CL reveal a complex oscillatory zonation, without any evidence of an inherited core boundary. Although the CL heterogeneity patterns of the zircons are variable, the typical characteristics for zircons that experienced multi-stage histories are not obvious.

All results yielded two age groups. Group A yielded highly scattered ages, from 169 to 2740 Ma (Figure 4A), which have almost no geological significance. The uranium contents of the group B are between 388 and 2164 ppm. Their $^{206}Pb/^{204}Pb$ ratios are between 1706 and 15268.

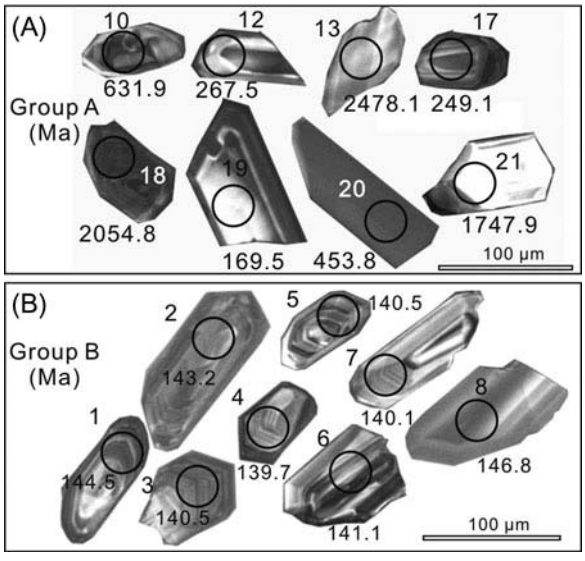

Figure 3. Representative cathodoluminescence (CL) images of older zircons (group A) revealing different, complex textures (A), and younger zircons (group B) showing the oscillatory zone (B) in the quartz–chalcopyrite–pyrite veins from the Yinjiagou deposit.

Eight spots yielded a weighted mean $^{206}Pb/^{238}U$ age of 142.0 ± 1.5 Ma (Figure 4B) (95% confidence limits, MSWD = 1.4).

Re–Os dating of pyrite

Blank-corrected Re and Os data and isotopic ratios for six pyrite samples from the Yinjiagou deposit are presented in Table 2. Analyses of different fractions of two samples (HY3-7 and HY3-14) yielded reproducible results for both Re and Os but much less reproducible isotopic ratios. The total Os concentrations vary considerably (5.1–313.4 ppt) due to the contributions of radiogenic ^{187}Os, which make up 54–97% of the total Os budget. The common Os contents are rather low (0.5–20.1 ppt), and the widely varied Re contents (3.0–199.2 ppb) depend on the features of the fluids in the pyrite. The fluids of samples richest in Re and Os showed boiling features, whereas the fluid of samples with the lowest Re contained only liquid–vapour aqueous fluid inclusions (Zhu *et al*. 2013).

Stein *et al*. (2000) suggested that the best way to represent the results from the low-level highly radiogenic sulphides is to plot the radiogenic ^{187}Os against ^{187}Re rather than $^{187}Re/^{188}Os$ *versus* $^{187}Os/^{188}Os$, because ^{188}Os is poorly determined and can generally be accounted for by the blank. Contrary to the assertions of Stein *et al*. (2000), reliable geochronological and tracer information has been obtained using the $^{187}Re/^{188}Os$ *versus* $^{187}Os/^{188}Os$ isochron plots. For example, Barra *et al*. (2002) obtained a similar age from pyrite samples compared with the molybdenite ages; Zhang *et al*. (2005) found that the ages of pyrite from both plotting techniques are close to the error. In this text, the regression of the blank-corrected $^{187}Re/^{188}Os$ and $^{187}Os/^{188}Os$ ($n = 6$) data yielded a model 1 Re–Os age of 142.3 ± 3.0 Ma, with an initial $^{187}Os/^{188}Os$ of 0.14 ± 0.23 (MSWD = 1.01, Figure 4C), which is similar to another model 1 Re–Os age of 141.1 ± 1.1 Ma plotted on the ^{187}Os *versus* ^{187}Re correlation diagram (MSWD = 0.58, Figure 4D) in the error limit. Hence, we suggest that 141 Ma best represents the age of the main stage chalcopyrite–pyrite mineralization at the Yinjiagou deposit.

Discussion

Genesis of the Group B zircons

The genesis of zircons is a significant research field that is crucial to understanding the behaviour of zircon in the magmatic–hydrothermal processes and to interpreting the U–Pb ages. However, up to now, no strict criterion has existed to distinguish among the hydrothermal, magmatic, and metamorphic zircons up to now. Hoskin and Schaltegger (2003) have summarized both the textural and compositional characteristics of hydrothermal zircons in

Table 1. U–Pb isotopic data of zircons from the quratz–chalcopyrite–pyrite veins of the Yinjiagou deposit.

	Isotopic ratios						Age (Ma)						Concentration (ppm)			
No.	$^{207}Pb/^{206}Pb$	1σ	$^{207}Pb/^{235}U$	1σ	$^{206}Pb/^{238}U$	1σ	$^{207}Pb/^{206}Pb$	1σ	$^{207}Pb/^{235}U$	1σ	$^{206}Pb/^{238}U$	1σ	U	Th	Pb	Th/U
Younger zircons																
1	0.0480	0.0030	0.1499	0.0030	0.0227	0.0030	97.1	31.6	141.8	2.7	144.5	2.1	1634	1208	47	0.74
2	0.0488	0.0029	0.1511	0.0029	0.0225	0.0029	136.6	26.8	142.9	2.5	143.2	2.1	2164	505	54	0.23
3	0.0478	0.0042	0.1452	0.0042	0.0220	0.0042	88.5	57.3	137.7	3.7	140.5	2.1	1184	1762	39	1.49
4	0.0476	0.0054	0.1438	0.0054	0.0219	0.0054	79.6	80.2	136.4	4.8	139.7	2.1	808	966	25	1.20
5	0.0484	0.0045	0.1471	0.0045	0.0220	0.0045	120.0	62.1	139.4	4.0	140.5	2.1	607	733	19	1.21
6	0.0476	0.0051	0.1453	0.0051	0.0221	0.0051	81.0	72.8	137.8	4.5	141.1	2.1	450	453	14	1.01
7	0.0495	0.0052	0.1501	0.0052	0.0220	0.0052	173.2	71.5	142.0	4.6	140.1	2.1	388	292	11	0.75
8	0.0489	0.0037	0.1553	0.0037	0.0230	0.0037	143.2	42.9	146.6	3.3	146.8	2.2	1390	3660	60	2.63
Older zircons																
9	0.1107	0.0860	4.9260	0.0860	0.3227	0.0860	1811.3	13.3	1806.7	14.8	1802.7	24.9	310	84	119	0.27
10	0.0606	0.0153	0.8606	0.0153	0.1030	0.0153	625.3	19.7	630.4	8.4	631.9	9.2	487	634	73	1.30
11	0.0500	0.0078	0.2851	0.0078	0.0414	0.0078	194.8	52.3	254.7	6.2	261.2	3.8	330	170	17	0.51
12	0.0506	0.0089	0.2957	0.0089	0.0424	0.0089	223.8	58.8	263.1	7.0	267.5	3.9	306	185	16	0.60
13	0.1665	0.1730	10.7597	0.1730	0.4688	0.1730	2522.5	9.1	2502.6	15.0	2478.1	31.2	111	79	71	0.71
14	0.1557	0.2383	7.5208	0.2383	0.3503	0.2383	2409.4	16.4	2175.5	28.8	1936.2	50.6	648	344	295	0.53
15	0.1882	0.2121	13.7490	0.2121	0.5297	0.2121	2726.8	5.6	2732.6	14.7	2740.4	33.7	435	194	299	0.45
16	0.1172	0.0936	5.4624	0.0936	0.3380	0.0936	1914.1	14.8	1894.7	14.8	1877.0	24.5	198	40	78	0.20
17	0.0510	0.0068	0.2775	0.0068	0.0395	0.0068	240.9	44.5	248.6	5.5	249.5	3.7	414	329	21	0.79
18	0.1601	0.1300	8.2852	0.1300	0.3754	0.1300	2456.3	7.6	2262.7	14.3	2054.8	26.5	248	307	140	1.24
19	0.0509	0.0081	0.1868	0.0081	0.0266	0.0081	234.1	91.2	173.9	7.0	169.5	2.6	608	406	21	0.67
20	0.0559	0.0097	0.5625	0.0080	0.0729	0.0072	450.1	24.1	453.1	6.8	453.8	6.6	915	462	81	0.50
21	0.1073	0.0846	4.6080	0.0846	0.3115	0.0846	1754.1	19.0	1750.7	15.4	1747.9	23.2	84	76	35	0.91

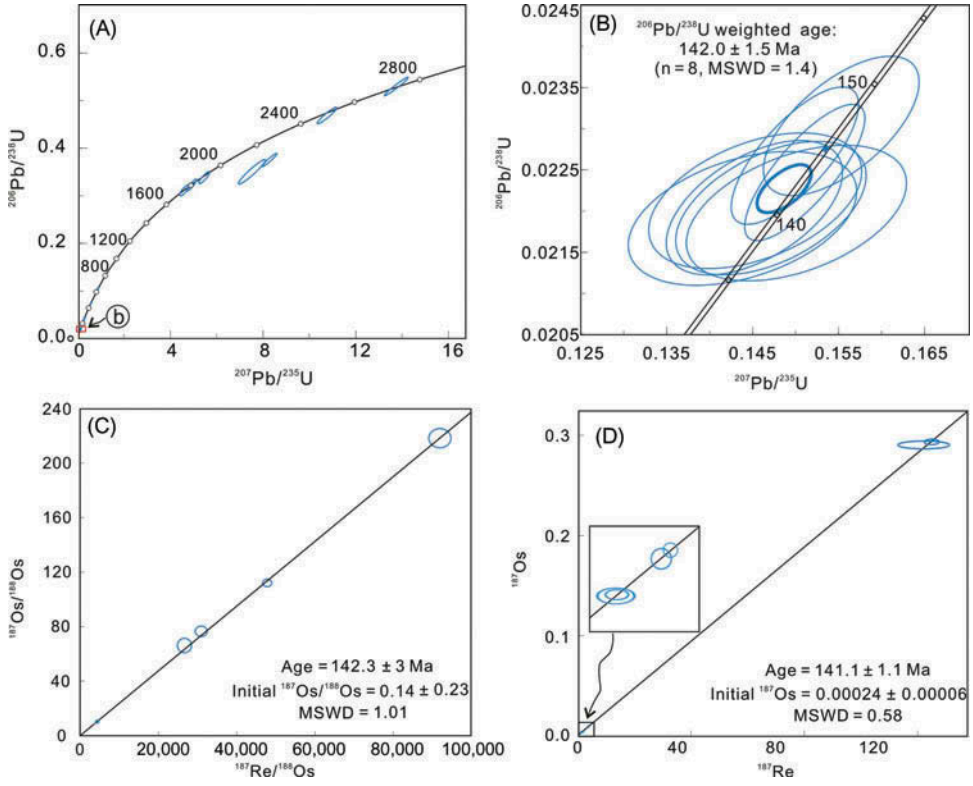

Figure 4. U–Pb concordia diagrams for zircons in the quartz–chalcopyrite–pyrite veins (A and B) and Re–Os isochron plots for pyrite samples (C and D) from the Yinjiagou deposit.

Table 2. Re–Os isotopic data of pyrite samples from the Yinjiagou deposit.

Sample	Re (ppb)	2σ	^{187}Re (ppb)	2σ	Os total (ppb)	2σ	^{187}Os (ppb)	2σ	^{187}Re/^{188}Os	2σ	^{187}Os/^{188}Os	2σ
HY3-7-1	6.4	0.1	4.0	0.07	0.0166	0.0008	0.0096	0.0003	4283	351	10.3	0.9
HY3-7-2	6.6	0.0	4.1	0.03	0.0186	0.0002	0.0100	0.0001	3611	37	8.7	0.1
HY3-11	194.8	1.5	122.4	0.96	0.3007	0.0034	0.2907	0.0032	91923	2315	218.2	5.8
HY3-12	199.2	1.4	125.2	0.86	0.3134	0.0026	0.2937	0.0023	47756	946	112.0	2.3
HY3-14-1	3.0	0.0	1.9	0.02	0.0051	0.0001	0.0046	0.0000	30876	1264	76.6	3.1
HY3-14-2	3.0	0.0	1.9	0.02	0.0052	0.0002	0.0047	0.0002	26588	1470	66.1	4.3

Notes: All data are blank corrected; blanks for Re and Os were 0.2 ± 0.6 pg and 0.22 ± 0.1 pg, respectively, with an average ^{187}Os/^{188}Os value of 0.2 ± 0.06; all uncertainties are determined by error propagation of uncertainties in Re and Os mass spectrometer measurements, blank abundances and isotopic compositions, and spike calibrations.

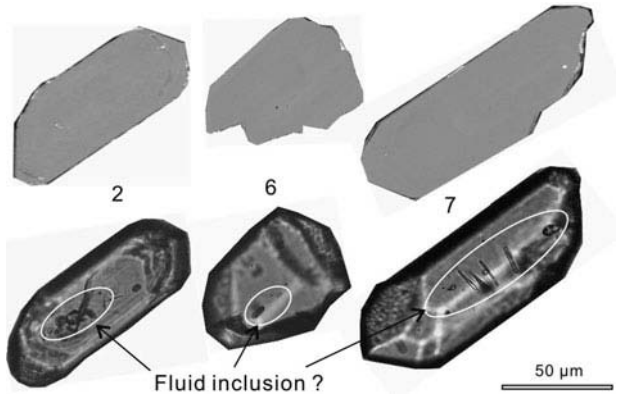

Figure 5. Back-scattered electron (BSE) (above) and transmitted (below) images of younger zircons (group B).

the literatures and concluded that the characteristics are not definitive (Pettke *et al*. 2005). Hoskin (2005) suggested that the trace-element compositions of the hydrothermal and magmatic zircon are distinct, yet Fu *et al*. (2009) considered that the rare-earth elements patterns of hydrothermal and magmatic zircons were most likely distinctive only in certain individual cases.

The group B zircons consist of a low-CL central portion, followed by a relatively undisturbed oscillatory zone. The oscillatory zone is quite common within igneous zircons and may represent multiple or single petrogenetic events (Hoskin and Schaltegger 2003). By comparison, rare documented examples of hydrothermal zircons are reported to occur as oscillatory zones (Pettke *et al*. 2005; Lawrie *et al*. 2007). Schaltegger (2007) also noted that zircon precipitated from a fluid or fluid-saturated melt might exhibit coherent internal structures with oscillatory or sector zoning and those so-called hydrothermal zircons, without exception, contain either secondary domains around/cutting across primary growth zones or hydrothermal mineral inclusions. The BSE images of the group B zircons did not reveal their compositional variability (above images of Figure 5), indicating no trapped mineral inclusions trapped and confirming their single-stage formation.

Another diagnostic argument is the fluid inclusions hosted in zircon that denotes the physical–chemical features of the hydrothermal fluid. Several publications have reported the P–T conditions of the fluid inclusions in the hydrothermal zircons (Dubińska *et al*. 2004; Lawrie *et al*. 2007) and certain researchers identified the fluid inclusions in zircon from morphology or laser Raman analysis (Claoué-Long *et al*. 1990; Kerrich and King 1993; Hu *et al*. 2004; Wan *et al*. 2012). Three of the eight group B zircons contain morphological-like fluid inclusions (below images of Figure 5). Nevertheless, laser Raman analysis indicates that the peak values of these portions are identical to those of zircons. Hence, these materials may be only cavities of zircon rather than fluid inclusions.

Additionally, the Th/U ratios from zircon analysis are between 0.23 and 2.63 as commonly seen in magmatic zircons, whereas the hydrothermal zircons frequently show more extreme values. Therefore, this evidence of the oscillatory growth zones and homogeneous compositions and the absence of mineral and fluid inclusions indicate that the group B zircons are most likely magmatic origin and are most likely sourced from another magmatic event. However, the hydrothermal genesis of certain zircons, such as No. 6 and No. 8, could not be exactly excluded and require further study. The magmatic origin of the group B zircons indicates that the age of the chalcopyrite–pyrite mineralization cannot exceed 142 Ma.

Source of the metals

Nearly all of the samples examined in this study have highly radiogenic Os compositions. Therefore, the initial ^{187}Os/^{188}Os of 0.14 ± 0.23 is relatively unreliable, with large uncertainties due to the scatter of ages in the regression line. The exceptions may be HY3-7-1 and HY3-7-2, which have relatively low measured ^{187}Os/^{188}Os ratios (Cardon *et al*. 2008). Assuming that these samples have an age of 141 Ma as calculated from Re–Os methods, this result implies that the initial ^{187}Os/^{188}Os ratio ranged between 0.11 and 0.16, which is close to that of the chondritic ^{187}Os/^{188}Os ratio of 0.13 at 141 Ma. Although the

initial ratio is poorly constrained, the clear approach from a mantle value indicates a significant mantle component for the source of the metals. This observation is also consistent with the high $^{3}He/^{4}He$ ratios (0.8–5.26 Ra, Ra = 1.39×10^{-6} for air) in pyrite from the Yinjiagou deposit (Zhu *et al*. 2013). These data indicate that the chalcopyrite–pyrite mineralization at the Yinjiagou deposit was introduced with the Late Cretaceous magmatism involving significant mantle materials.

Variations in the Re and Os concentrations

The Re enrichment in low-level highly radiogenic sulphides has been described by Ruiz *et al*. (1995), who found that the Re content in primary chalcocite is below the detection limits, whereas secondary (supergene) chalcocite can contain up to 10 ppm Re. Morelli *et al*. (2004) considered that the high variability of Re may reflect variations in fluid chemistry or may derive from different sources. Based on their experimental studies, Xiong *et al*. (2006) suggested that Re can be leached and transported downward under supergene conditions and subsequently re-deposited in the reduced zone of the supergene environments, thus producing considerable Re enrichment. Cardon *et al*. (2008) observed that Re is considerably enriched in the apex zone of the porphyry, which could be explained by intensive boiling.

The Re contents (and thus the total Os contents) in the analysed samples vary largely depending on the fluid features. Fluid inclusions trapped in high-Re pyrite have been observed that vary in composition from vapour-rich and liquid-rich, to halite-bearing only within single inclusion planes (Zhu *et al*. 2013). Such features are commonly considered to indicate boiling (Bodnar 1985), which would have been accompanied by elemental partitioning between the liquid (chlorides) and vapour phases (volatile compounds), e.g. the Fe element, which preferentially enters the hyper-saline liquid during boiling (Heinrich *et al*. 1999; Seo *et al*. 2009; Zhu *et al*. 2013). Xiong and Wood (1999) found that Re is concentrated in chloride-rich fluids as Re-chloride complexes in high-temperature environments under near-porphyry copper hydrothermal systems. Under such boiling conditions, Re is concentrated in chloride-rich fluids via Re-chloride complexes. Hence, it is possible that the boiling could have resulted in the fractionation and increase of Re.

Time and genesis of poly-metallic mineralization

An accurate geochronology contributes to understanding of the timing relationships and permits refinement of the genetic model. The longevity of hydrothermal systems is one of the fundamental questions in metallogenesis. Certain researchers have proposed that in special circumstances, hydrothermal circulation may occur during a rather short time of less than 1 million years after a single intrusive event (Cathles *et al*. 1997; Marsh *et al*. 1997; Stein and Markey 2006). However, other deposits are recognizably the result of multiple magmatic and hydrothermal events. Studies have shown that the main period of ore formation may post-date the emplacement of the hosting pluton by several to tens of millions of years (Chesley 1999; Kendrick *et al*. 2001).

A combination of geological and isotopic data, together with the results of this study, constrains the multiple magmatic and hydrothermal events in the Yinjiagou deposit. Precious U–Pb chronology indicates that at least two episodes of magmatic invasion occurred in this district, one that formed granite and diorite porphyries and another that yielded veined biotite ivernite (Figure 1). The veinlet molybdenite occurs within the KGP, with molybdenite Re–Os ages between 145 and 148 Ma (Wu 2011), representing the early porphyry mineralization. The chalcopyrite–pyrite mineralization is located in the KGP and QDP, and the mineralization age is defined as 141 Ma in this study. This main mineralization may be related to the hydrothermal activity of a deeper intrusion, despite the fact that the superficial occurrence of this magmatic event is inconspicuous. Intrusion of younger granites hidden beneath the current level of exposure may have provided fluids for a discrete and later magmatic-hydrothermal event. Therefore, a multi-stage model for the introduction of pyrite is favoured over a single climactic poly-metallic mineralization event. The main chalcopyrite–pyrite mineralization occurred late in the magmatic history of the district and overlapped the hydrothermal systems.

Previous isotopic, geochemical, and fluid inclusion evidence indicates that the fluid source of the Late Jurassic–Early Cretaceous deposits in the SMNCC is mainly derived from granitic magma locally mixed with meteoric water (e.g. Li *et al*. 2007; Chen *et al*. 2009; Mao *et al*. 2011, and references therein). The occurrences of porphyry (skarn) Mo deposits and the outlying poly-metallic veins at the deposit scale may belong to the same ore system (Mao *et al*. 2009). This large-scale metallogenesis in the SMNCC is related to a series of Mesozoic granitoid plutons triggered by the transformation of the tectonic regime and formed in an extensional setting (e.g. Ratschbacher *et al*. 2003; Mao *et al*. 2008; Ling *et al*. 2009; Li *et al*. 2012). Considering the metallogenesis domains, this extension is reflected by the dominant mantle-derived fluids involved in the poly-metallic mineralization as supported by this study and other S–He–Ar analysis (Zhu *et al*. 2009; Li *et al*. 2013a). The chalcopyrite–pyrite mineralization of the Yinjiagou deposit indicates an intense extensional setting, which might belong to the Early Cretaceous lithospheric destruction and thinning (Wu *et al*. 2008; Zhu *et al*. 2011; Li *et al*. 2012) of the SMNCC.

Conclusions

This study demonstrates that the radiometric timing of chalcopyrite–pyrite mineralization places certain constraints on the theories of ore genesis. Our discovery of magmatic zircons trapped in the quartz–chalcopyrite–pyrite veins successfully defines the time of pyrite precipitation to less than 142 Ma despite the fact that this age could not be distinguished from the pyrite Re–Os age within error limits. Pyrite Re–Os dating documents the age of chalcopyrite–pyrite to 141 Ma, and the extreme rhenium enrichment could be explained by intensive boiling. The low initial $^{187}Os/^{188}Os$ of the least radiogenic sample suggests a dominant mantle origin for the metals, indicating that a later hidden magmatic intrusion involving an excess of mantle materials might account for this hydrothermal system and thus for the chalcopyrite–pyrite deposits.

Acknowledgements

We thank Xianhua Li, Qiuli Li, and Guoqiang Tang for their technical support during the analytical work. Thoughtful suggestions by Editor W.G. Ernst and reviewer Z.Q. Hou greatly helped to improve the article. This research was funded jointly by the National Basic Research Programme (No. 2012CB416601) and NSFC grants (No. 41202066). M.T. Zhu is grateful for the support from the China Postdoctoral Science Foundation grant (No. 2011M500386).

References

Arne, D.C., Bierlin, F.P., Morgan, J.W., and Stein, H.J., 2001, Re-Os dating of sulfides associated with gold mineralization in Central Victoria, Australia: Economic Geology, v. 96, p. 1455–1459.

Barra, F., Ruiz, J., Mathur, R., and Titley, S., 2002, A Re–Os study of sulfide minerals from the Bagdad porphyry Cu–Mo deposit, northern Arizona, USA: Mineralium Deposita, v. 38, p. 585–596.

Bodnar, R.J., 1985, Fluid inclusion systematics in epithermal systems: Reviews in Economic Geology, v. 2, p. 73–97.

Cardon, O., Reisberg, L., Andre-Mayer, A.-S., Leroy, J., Milu, V., and Zimmermann, C., 2008, Re-Os systematics of pyrite from the Bolcana porphyry copper deposit, Apuseni mountains, Romania: Economic Geology, v. 103, p. 1695–1702.

Cathles, L.M., Erendi, A.H.J., and Barrie, T., 1997, How long can a hydrothermal system be sustained by a single intrusive event?: Economic Geology, v. 92, p. 766–771.

Chen, Y.J., and Fu, S.G., 1992, Mineralization of gold deposits in West Henan, China: Beijing, Chinese Seismological Press, 234 p. (in Chinese).

Chen, Y.J., Pirajno, F., Li, N., Guo, D.S., and Lai, Y., 2009, Isotope systematics and fluid inclusion studies of the Qiyugou breccia pipe-hosted gold deposit, Qinling Orogen, Henan province, China: Implications for ore genesis: Ore Geology Reviews, v. 35, p. 245–261.

Cherniak, D.J., and Watson, E.B., 2001, Pb diffusion in zircon: Chemical Geology, v. 172, p. 5–24.

Chesley, J., 1999, Integrative geochronology of ore deposits: New insights into the duration and timing of hydrothermal circulation. In: Lambert, D.D., and Ruiz, J. (eds) Application of radiogenic isotopes to ore deposit research and exploration: Review Economic Geology, v. 12, p. 115–141.

Claoué-Long, J.C., King, R.W., and Kerrich, R., 1990, Archaean hydrothermal zircon in the Abitibi greenstone belt: Constraints on the timing of gold mineralisation: Earth and Planetary Science Letters, v. 98, p. 109–128.

Dubińska, E., Bylina, P., Kozłowski, A., Dörr, W., Nejbert, K., Schastok, J., and Kulicki, C., 2004, U–Pb dating of serpentinization: hydrothermal zircon from a metasomatic rodingite shell (Sudetic ophiolite, SW Poland): Chemical Geology, v. 203, p. 183–203.

Feng, C., Qu, W., Zhang, D., Dang, X., Du, A., Li, D., and She, H., 2009, Re–Os dating of pyrite from the Tuolugou stratabound Co(Au) deposit, eastern Kunlun Orogenic Belt, northwestern China: Ore Geology Reviews, v. 36, p. 213–220.

Fu, B., Mernagh, T.P., Kita, N.T., Kemp, A.I.S., and Valley, J.W., 2009, Distinguishing magmatic zircon from hydrothermal zircon: A case study from the Gidginbung high-sulphidation Au–Ag–(Cu) deposit, SE Australia: Chemical Geology, v. 259, p. 131–142.

Heinrich, C.A., Gunther, D., Audetat, A., Ulrich, T., and Frischknecht, R., 1999, Metal fractionation between magmatic brine and vapor, determined by microanalysis of fluid inclusions: Geology, v. 27, p. 755–758.

Hoskin, P.W.O., 2005, Trace-element composition of hydrothermal zircon and the alteration of Hadean zircon from the Jack Hills, Australia: Geochimica et Cosmochimica Acta, v. 69, p. 637–648.

Hoskin, P.W.O., and Schaltegger, U., 2003, The composition of zircon and igneous and metamorphic petrogenesis: Reviews in Mineralogy and Geochemistry, v. 53, p. 27–62.

Hu, F.F., Fan, H.R., Yang, J.H., Wan, Y.S., Liu, D.Y., Zhai, M.G., and Jin, C.W., 2004. Mineralizing age of the Rushan lode gold deposit in the Jiaodong Peninsula: SHRIMP U–Pb dating on hydrothermal zircon. Chinese Science Bulletin, v. 49, p. 1629–1636.

Jin, X.D., Li, W.J., Wu, H.Y., Zhang, L.C., and Du, A.D., 2010, Development of Re–Os isotopic dating analytical technique and determination know-how on ICP-MS precise dating for molybdenite: Acta Petrologica Sinica, v. 26, p. 1617–1624 (in Chinese with English abstract).

Kendrick, M.A., Burgess, R., Pattrick, R.A.D., and Turner, G., 2001, Halogen and Ar–Ar age determinations of inclusions within quartz veins from porphyry copper deposits using complementary noble gas extraction techniques: Chemical Geology, v. 177, p. 351–370.

Kerrich, R., and King, R., 1993, Hydrothermal zircon and baddeleyite in Val-d'Or Archean mesothermal gold deposits: Characteristics, compositions, and fluid-inclusion properties, with implications for timing of primary gold mineralization: Canadian Journal of Earth Sciences, v. 30,p. 2334–2351.

Kirk, J., Ruiz, J., Chesley, J., Walshe, J., and England, G., 2002, A major Archean, gold- and crust-forming event in the Kaapvaal Craton, South Africa: Science, v. 297, p. 1856–1858.

Lawrie, K.C., Mernagh, T.P., Ryan, C.G., Achterbergh, E.V., and Black, L.P., 2007, Chemical fingerprinting of hydrothermal zircons: An example from the Gidginbung high sulphidation Au–Ag–(Cu) deposit, New South Wales, Australia: Proceedings of the Geologists' Association, v. 118, p. 37–46.

Lee, J.K.W., Williams, I.S., and Ellis, D.J., 1997, Pb, U and Th diffusion in natural zircon: Nature, v. 390, p. 159–162.

Li, J.J., Shen, B.F., Mao, D.B., Li, S.B., Zhou, H.F., and Cheng, Y.M., 1997, Mineralization ages of the Jiapigou gold deposits, Jilin: Acta Geologica Sinica – English Edition, v. 71, p. 180–188.

Li, J.-W., Bi, S.-J., Selby, D., Chen, L., Vasconcelos, P., Thiede, D., Zhou, M.-F., Zhao, X.-F., Li, Z.-K., and Qiu, H.-N., 2012, Giant Mesozoic gold provinces related to the destruction of the North China Craton: Earth and Planetary Science Letters, v. 349–350, p. 26–37.

Li, N., Chen, Y.J., Zhang, H., Zhao, T.P., Deng, X.H., Wang, Y., and Ni, Z.Y., 2007, Molybdenum deposits in East Qinling: Earth Science Frontiers, v. 14, p. 186–198 (in Chinese with English abstract).

Li, Q.L., Li, X.H., Liu, Y., Tang, G.Q., Yang, J.H., and Zhu, W.G., 2010, Precise U–Pb and Pb–Pb dating of Phanerozoic baddeleyite by SIMS with oxygen flooding technique: Journal of Analytical Atomic Spectrometry, v. 25, p. 1107–1113.

Li, S.R., Santosh, M., Zhang, H., Shen, J., Dong, G., Wang, J., and Zhang, J., 2013a, Inhomogeneous lithospheric thinning in the central North China Craton: Zircon U-Pb and S-He-Ar isotopic record from magmatism and metallogeny in the Taihang Mountains: Gondwana Research, v. 23, p. 141–160.

Li, T.G., Wu, G., Chen, Y.C., Li, Z.Y., and Yang, X.S., 2013b, Geochronology, geochemistry and petrogenesis of the Yinjiagou complex in western Henan Province, China: Acta Petrologica Sinica, v. 29, p. 46–66 (in Chinese with English abstract).

Ling, M.-X., Wang, F.-Y., Ding, X., Hu, Y.-H., Zhou, J.-B., Zartman, R.E., Yang, X.-Y., and Sun, W., 2009, Cretaceous ridge subduction along the lower Yangtze River Belt, Eastern China: Economic Geology, v. 104, p. 303–321.

Lu, X.X., Yu, Z.P., Feng, Y.L., Wang, Y.T., Ma, W.F., and Cui, H.F., 2002, Mineralization and tectonic setting of deep-hypabyssal granites in East Qinling Mountain: Mineral Deposits, v. 21, p. 168–178 (in Chinese with English abstract).

Ludwig, K.R., 2003, ISOPLOT 3.0—A geochronological toolkit for Microsoft Excel: Berkeley Geochronology Center Special Publication, 70 pp.

Mao, J.W., Pirajno, F., Xiang, J.F., Gao, J.J., Ye, H.S., Li, Y.F., and Guo, B.J., 2011, Mesozoic molybdenum deposits in the East Qinling–Dabie Orogenic Belt: Characteristics and tectonic settings: Ore Geology Reviews, v. 43, p. 264–293.

Mao, J.W., Xie, G.Q., Bierlein, F., Qü, W.J., Du, A.D., Ye, H.S., Pirajno, F., Li, H.M., Guo, B.J., Li, Y.F., and Yang, Z.Q., 2008, Tectonic implications from Re–Os dating of Mesozoic molybdenum deposits in the East Qinling–Dabie Orogenic Belt: Geochimica et Cosmochimica Acta, v. 72, p. 4607–4626.

Mao, J.W., Ye, H.S., Wang, R.T., Dai, J.Z., Jian, W., Xiang, J.F., Zhou, K., and Meng, F., 2009, Mineral deposit model of Mesozoic porphyry Mo and vein type Pb-Zn-Ag ore deposits in the East Qinling, Central China and its implication for prospecting: Geological Bulletin of China, v. 29, p. 72–79 (in Chinese with English abstract).

Marsh, T.M., Einaudi, M.T., and McWilliams, M., 1997, $^{40}Ar/^{39}Ar$ geochronology of Cu-Au and Au-Ag mineralization in the Potrerillos District, Chile: Economic Geology, v. 92, p. 784–806.

Mathur, R., Ruiz, J., and Tornos, F., 1999, Age and sources of the ore at Tharsis and Rio Tinto, Iberian Pyrite Belt, from Re-Os isotopes: Mineralium Deposita, v. 34, p. 790–793.

Morelli, R.M., Creaser, R.A., Selby, D., Kelley, K.D., Leach, D.L., and King, A.R., 2004, Re-Os sulfide geochronology of the red dog sediment-hosted Zn-Pb-Ag deposit, Brooks Range, Alaska: Economic Geology, v. 99, p. 1569–1576.

Pelleter, E., Cheilletz, A., Gasquet, D., Mouttaqi, A., Annich, M., El Hakour, A., Deloule, E., and Féraud, G., 2007, Hydrothermal zircons: A tool for ion microprobe U–Pb dating of gold mineralization (Tamlalt–Menhouhou gold deposit—Morocco): Chemical Geology, v. 245, p. 135–161.

Pettke, T., Audétat, A., Schaltegger, U., and Heinrich, C.A., 2005, Magmatic-to-hydrothermal crystallization in the W–Sn mineralized Mole Granite (NSW, Australia): Part II: Evolving zircon and thorite trace element chemistry: Chemical Geology, v. 220, p. 191–213.

Ratschbacher, L., Hacker, B.R., Calvert, A., Webb, L.E., Grimmer, J.C., McWilliams, M.O., Ireland, T., Dong, S., and Hu, J., 2003, Tectonics of the Qinling (Central China): Tectonostratigraphy, geochronology, and deformation history: Tectonophysics, v. 366, p. 1–53.

Rubin, J.N., Henry, C.D., and Price, J.G., 1989, Hydrothermal zircons and zircon overgrowths, Sierra Blanca Peaks, Texas: American Mineralogist, v. 74, p. 865–869.

Ruiz, J., McCandless, T., Baker, M., Chesley, J., Puig, A., and Munizaga, F., 1995, Dating of supergene enrichment by Re–Os isotopes [abs.]: Geological Society of America Abstracts with Programs, v. 27, p. 467.

Schaltegger, U., 2007, Hydrothermal Zircon: Elements, v. 3, p. 51–79.

Selby, D., Creaser, R.A., Hart, C.J.R., Rombach, C.S., Thompson, J.F.H., Smith, M.T., Bakke, A.A., and Goldfarb, R.J., 2002, Absolute timing of sulfide and gold mineralization: A comparison of Re-Os molybdenite and Ar-Ar mica methods from the Tintina Gold Belt, Alaska: Geology, v. 30, p. 791–794.

Seo, J.H., Guillong, M., and Heinrich, C.A., 2009, The role of sulfur in the formation of magmatic-hydrothermal copper-gold deposits: Earth and Planetary Science Letters, v. 282, p. 323–328.

Stein, H., and Markey, R., 2006, Timescales for fluid storage and release in porphyry Cu-Mo systems – Timescales for felsic magma storage and volcanic eruptions: Geochimica et Cosmochimica Acta, v. 70, p. A613.

Stein, H.J., Markey, R.J., Morgan, J.W., Hannah, J.L., and Scherstén, A., 2001, The remarkable Re–Os chronometer in molybdenite: How and why it works: Terra Nova, v. 13, p. 479–486.

Stein, H.J., Morgan, J.W., and Scherstén, A., 2000, Re-Os dating of low-level highly radiogenic (LLHR) sulfides: The Harnäs gold deposit, Southwest Sweden, Records Continental-Scale Tectonic Events: Economic Geology, v. 95, p. 1657–1671.

Stein, H.J., Sundblad, K., Markey, R.J., Morgan, J.W., and Motuza, G., 1998, Re-Os ages for Archean molybdenite and pyrite, Kuittila-Kivisuo, Finland and Proterozoic molybdenite, Kabeliai, Lithuania: Testing the chronometer in a metamorphic and metasomatic setting: Mineralium Deposita, v. 33, p. 329–345.

Wan, B., Xiao, W., Zhang, L., and Han, C., 2012, Iron mineralization associated with a major strike–slip shear zone: Radiometric and oxygen isotope evidence from the Mengku deposit, NW China: Ore Geology Reviews, v. 44, p. 136–147.

Wu, F.Y., Xu, Y.G., Gao, S., and Zheng, J.P., 2008, Lithospheric thinning and destruction of the North China Craton: Acta Petrologica Sinica, v. 24, p. 1145–1174 (in Chinese with English abstract).

Wu, G., 2011, Polymetallic metallogenic regularity and prognosis studies of the Yinjiagou area, Henan Province: Unpub. Post Doctorate Outbound Report thesis, Institute of Mineral Resources, Chinese Academy of Geological Sciences.

Wu, H., Zhang, L., Wan, B., Chen, Z., Xiang, P., Pirajno, F., Du, A., and Qu, W., 2011, Re–Os and $^{40}Ar/^{39}Ar$ ages of the Jiguanshan porphyry Mo deposit, Xilamulun metallogenic belt, NE China, and constraints on mineralization events: Mineralium Deposita, v. 46, p. 171–185.

Xiong, Y., and Wood, S.A., 1999, Experimental determination of the solubility of ReO_2 and the dominant oxidation state of rhenium in hydrothermal solutions: Chemical Geology, v. 158, p. 245–256.

Xiong, Y., Wood, S., and Kruszewski, J., 2006, Hydrothermal transport and deposition of rhenium under subcritical conditions revisited: Economic Geology, v. 101, p. 471–478.

Zhang, G., Zhang, B., Yuan, X., and Chen, J., 2001, Qinling orogenic belt and continental dynamics: Beijing, Science Press, 855 p. (in Chinese).

Zhang, L.C., Xiao, W.J., Qin, K.Z., Qu, W.J., and Du, A.D., 2005, Re–Os isotopic dating of molybdenite and pyrite in the Baishan Mo–Re deposit, eastern Tianshan, NW China, and its geological significance: Mineralium Deposita, v. 39, p. 960–969.

Zhang, X.M., Qiao, C.J., Cai, X.D., Zhang, X.W., Wang, W.L., Zhang, C.H., and Zhang, Y.H., 2008, Characteristics of Yinjiagou polymetal-pyrite deposit related to pulse magmatic intrusions in Henan, China: Global Geology, v. 27, p. 137–145 (in Chinese with English abstract).

Zhu, L.M., Zhang, G.W., Guo, B., and Li, B., 2009, He–Ar isotopic system of fluid inclusions in pryite from the molybdenum deposits in south margin of North China Block and its trace to metallogenecit and geodynamic background: Chinese Science Bulletin, v. 54, p. 1725–1735.

Zhu, M.T., Zhang, L.C., Wu, G., He, H.Y., and Cui, M.L., 2013, Fluid inclusions and He–Ar isotopes in pyrite from the Yinjiagou deposit in the southern margin of the North China Craton: A mantle connection for poly-metallic mineralization: Chemical Geology (in press).

Zhu, R.X., Chen, L., Wu, F.Y., and Liu, J.L., 2011, Timing, scale and mechanism of the destruction of the North China Craton: Science China: Earch Science, v. 54, p. 789–797.